The effect of prepreg ply thickness in carbon fiber reinforced composites on intralaminar toughness and shear strength in cryogenic environments for liquid hydrogen storage tanks

Eduardo Szpoganicz [a], Fabian Hübner [b], Uwe Beier [b], Matthias Geistbeck [b], Holger Ruckdäschel [a,*]

[a] *Department of Polymer Engineering, University of Bayreuth, Bayreuth, Germany*
[b] *Airbus Central Research and Technology, Taufkirchen, Munich, Germany*

ARTICLE INFO

ABSTRACT

This study investigates the effect of prepreg ply thickness on the intralaminar toughness and shear strength of carbon-fiber reinforced polymer (CFRP) in room temperature and cryogenic environments. A toughened epoxy resin, optimized for ultra-low temperatures, was impregnated with unidirectional carbon-fibers at 45, 70, and 140 g/m^2 areal weights. The intralaminar energy release rates in modes I and II, along with the interlaminar shear strength, were evaluated under liquid nitrogen (*in-situ*) testing conditions to assess the performance of these composites in cryogenics. Optical and scanning electron microscopy correlated fiber-matrix distribution and regularity with failure modes and performance. While G_{IC} decreased from 296 K to 77 K, ILSS was notably higher in cryogenic environments. Both intralaminar toughness and interlaminar strength were improved by thinner plies, especially at 77 K. Thus, highlighting the importance of fiber-matrix uniformity in optimizing delamination and shear properties under cryogenic conditions, where sensitivity to irregularities increases.

1. Introduction

Hydrogen fuel is gaining attention for its potential to reduce CO2 emissions across various transportation sectors, which together can contribute up to 17–18 % of global energy-related emissions [1]. Liquid hydrogen (LH2) offers a significantly higher energy density by volume compared to gaseous hydrogen, making it appealing for the standard jet-fuel transitioning in aviation by potentially maintaining flight range and operational capabilities while significantly reducing in-flight CO2 emissions. Major aircraft manufacturers are actively developing technologies for hydrogen-powered commercial aircraft. However, the widespread adoption of LH2 faces challenges, especially in storage, necessitating materials that withstand extremely low temperatures and prevent hydrogen leakage [2]. LH2's lower volumetric energy density over fossil fuels requires larger storage volumes and thus larger tanks, making traditional metallic tanks less appealing. While carbon-fiber reinforced plastics (CFRPs) offer structural integrity and lightweight advantages, their performance in cryogenic temperatures is limited, posing integrity and leakage control challenges. Despite ongoing research efforts, the complex relationship between ultra-low temperature and CFRP failure behavior hinder material design and widespread adoption.

The lack of reliable failure criteria for CFRP laminates operating in cryogenics poses challenges for developing dedicated CFRP composites for LH2 storage tanks. This is especially true for epoxy systems, where molecular mobility and relaxation are significantly reduced, leading to embrittlement, particularly with common tougheners and organic-based additives [3–7].

Johnson et al. [8] first introduced the energy release rate mode I (G_{IC} test) in cryogenic environments for an aerospace application CFRP material. The work revealed the critical effect of the ultra-low temperature environment on the delamination toughness of the composite. Overall, the G_{IC} values were significantly lower at 77 K than at room temperature (RT). More recent works investigated the role of temperature on the different crack opening modes of glass-fiber fabric laminates [9–14]. These works reported that fatigue delamination growth rates of glass-fiber reinforced plastic (GFRP) woven laminates at 77 K and 4 K were lower than at RT. For instance, Miura et al. [10] investigated the
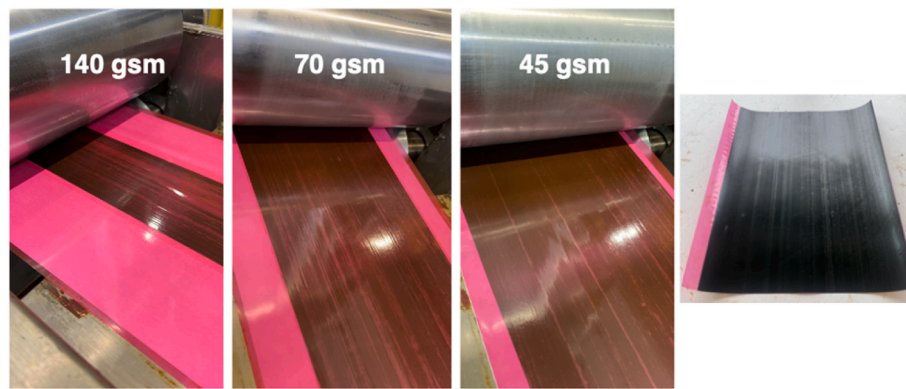
Fig. 1. Hot-melt prepreg manufacturing of CEP-IMA in different ply thicknesses.

cryogenic fatigue delamination behavior of GFRP under mode III loading. Here, a finite element analysis was implemented to calculate the energy release rate. Fatigue delamination growth rates in GFRP woven laminates are lower at 77 K and 4 K compared to RT, with a higher rate observed at 4 K than at 77 K, and the mechanisms driving fatigue delamination differ between cyclic and static conditions. In mode I fatigue crack growth in GFRP woven in cryogenic environments, Shindo et al. [12] developed an experimental and analytical study using compact tension specimens. Fatigue crack growth rates in woven laminates were reported as significantly lower at 77 K compared to RT, with fiber-matrix debonding and fiber pull-out dominating at high energy levels, while matrix cracking is predominant at low energy levels.

Similarly to the findings on static modulus and strength, the partially conflicting results and the reversal of changes in toughness parameters indicate that adverse microstructural effects are present simultaneously [3,4]. The fracture toughness of pure epoxy in cryogenic environments varies, with some studies showing increased fracture toughness (K_{IC}) at low temperatures [15–21], compared to RT. This variability is linked to lower chain mobility increasing intermolecular stiffness, thus improving matrix toughness. However, the absence of free-volume and mobility between molecules may suppress stress relaxation at the crack tip, potentially decreasing propagation energy. The combined effect here results in a complex analysis that can lead CFRP intralaminar delamination behavior in both directions.

The shear behavior of CFRP laminates is primarily influenced by the matrix properties. Under shear loading, the nonlinearity in the stress-strain response decreases with decreasing temperature [3,4]. This phenomenon is shown by Kumagai et al. [22], where RT fractography images express deeper cusps and larger deformations occur due to yielding, while at −100 °C smaller cusps in a higher density indicate microcracking accumulation followed by sudden failure. Only a few investigations carried out studies of the interlaminar shear strength (ILSS) in cold temperatures, once again focusing on glass-fiber wovens [23–25]. Nevertheless, the works proved that the rise in matrix stiffness by the colder temperatures increased the ILSS of the composite laminate.

Even though the major focus of the literature is attributed to the intrinsic properties of the matrix and CFRP composite, the acknowledgement that failure within CFRP laminates is highly influenced by the prepreg manufacturing and processing method is not mentioned. For a reasonable time, literature indicates that thinner-ply CFRP laminates exhibit improved mechanical performance due to reduced defects and irregularities resulting from prepreg manufacturing [26–29]. A novel processing method for spreading fiber tows to create thinner ply CFRP laminates was developed by Sihn et al. [28]. Their study explored the impact of reduced ply-thickness on the static and fatigue life of CFRP specimens tested at RT. The research revealed that thinner ply laminates alone effectively mitigate microcracking, delamination, and splitting damage under static, fatigue, and impact loads without the need for specialized resin. Similarly, Amacher et al. [29] reported comparable

findings, highlighting that the improved structural regularity, and reduced major defects in thinner-ply CFRP composites result in significantly enhanced mechanical performance. Notice, in cryogenic environments, the differing coefficient of thermal expansion (CTE) between fibers, resin, and ply-angle within the CFRP laminates creates residual stresses. While unidirectional (UD) composites experience minimal thermal stress due to uniform fiber orientation, multi-layer laminates with varied fiber angles face more significant stresses, potentially limiting their upscaled performance [3,4]. Additionally, the complexity of handling thin plies in production slows high-rate manufacturing, limiting their use in industry applications.

The aforementioned studies present remarkable enhancements of the CFRP material towards static and fatigue mechanical behavior, which would highly benefit composite failure progression for cryogenic structures by increasing shear strength and reducing crack propagation. However, these studies are mostly limited to RT environments and were not yet transferred to the cryogenic regime. Thus, in this study, the intralaminar toughness (mode I and II) and interlaminar shear strength of different ply thickness CFRP composites specifically designed for cryogenic environments were accessed at 77 K (*in-situ*). Optical and scanning electron microscopy (SEM) technologies were utilized to observe the structural difference between different ply-thickness laminates and the fractography involved in their cryogenic behavior. The damage process and overall performance was investigated and associated with the structure of the CFRP laminates resulting from the prepreg manufacturing. A strong correlation was found between the regularity of the laminate's structure and its intralaminar toughness and interlaminar strength at RT and 77 K.

2. Materials and methods

2.1. Prepreg material

For this study, a toughened epoxy resin designed to operate in cryogenic environments (CEP) was impregnated with 12K aerospace-grade unidirectional carbon-fibers HexTow® IMA (Hexcel Corporation, Stamford, USA). The CFRP material is referred to as CEP-IMA through this work. A particulate toughening agent Genioperl W36® (Wacker AG, Burghausen, Germany) was used in 5 vol% to 100 pt of the matrix mixture. The siloxane containing block-copolymeric toughener forms micelles core-shell structures in nanometer-sized domains. Further details about the cryogenic epoxy resin performance and development can be found in publications by Hübner et al. [19–21]. The prepreg material was impregnated in a hot-melt prepreg impregnation unit of Roth Composite Machinery GmbH (Steffenberg, Germany). Herein, CEP-IMA prepregs of different ply thicknesses (fiber areal weight of 45, 70 and 140 g/m^2 or gsm) were manufactured as a continuous unidirectional prepreg tape. Fig. 1 shows the prepreg tapes according to the fiber spreading areal weight. The aimed carbon-fiber

Table 1
Manufacturing parameters of the different ply thicknesses prepregs.

CEP-IMA prepreg system	Number of IMA spools	Roving spreading width (mm)	Prepreg thickness (μm)	Tape width (mm)
140 gsm	32	3.18	130–150	110
70 gsm	32	6.35	65–75	220
45 gsm	28	10.00	40–45	280

Table 2
Summarized parameters of different laminate systems to each according test.

Test	Laminate			
	Thickness	Fiber areal weight	Nr. of plies	FVC
G_{IC}	3.03 ± 0.12 mm	140 gsm	22	61 ± 4 %
G_{IIC}	2.94 ± 0.08 mm	70 gsm	44	60 ± 2 %
	3.08 ± 0.11 mm	45 gsm	66	59 ± 1 %
ILSS	2.02 ± 0.02 mm	140 gsm	16	60 ± 2 %
	1.82 ± 0.04 mm	70 gsm	24	62 ± 1 %
	2.04 ± 0.02 mm	45 gsm	44	60 ± 1 %

volume content (FVC) within the prepregs was 60 vol%. Individual details about their manufacturing parameters can be seen in Table 1. From the prepreg tapes, unidirectional laminates were manufactured through an autoclave process.

After consolidation, the laminates were scanned through an ultrasound pool scanner from Hillger NDT GmbH (Braunschweig, Germany). Overall, the CFRP plates did not exhibit signs of porosity or uneven regions. Subsequently, the laminates were cut into specimens by a rotating blade cutting machine Servocut 602 series from Metkon Instruments Inc. (Bursa, Turkey). The smooth and automated cut guaranteed no defects caused by the cutting process with a full parallel alignment along the length. The cutting blade contains a 400-mesh grit, which polishes the edges and ensures reduced stress concentration. Thermogravimetric analysis (TGA) was carried out using a TG 209 F1 Libra instrument from Netzsch-Geraetebau GmbH (Selb, Germany) to observe the FVC of the different laminates manufactured in this survey, according to DIN 16459:2019–12. See specific specimen details in Table 2.

2.2. Intralaminar toughness

Intralaminar energy release rate was measured for the composite laminates as mode I (G_{IC}) and mode II (G_{IIC}). For G_{IC} testing, double cantilever beam (DCB) specimens were tested according to DIN EN 6033. The test was carried out on a universal testing machine Zwick Z020, adapted with a double-walled tank for testing in liquid nitrogen (LN2). An illustrative and schematic image of the DCB testing setup can be seen in Fig. 2. A Teflon film is placed along one edge of the panel before processing to create an initial mid-plane delamination crack. Crack length of Mode I specimens started at 25 mm, and values were first taken at the length of 50 mm. The specimen is loaded constantly with a crosshead speed of 10 mm min^{-1} until a total crack length of about 110 mm has been achieved. At every 5 mm of crack length, a contrasting white paint applied to the specimen's longitudinal section (visible in LN2 under a magnifying glass) enabled conversion from crosshead displacement. The dewar here must be large enough so the crack length can be seen while the specimen is immersed in LN2 and transduced simultaneously within crosshead displacement. A Teflon spray was utilized to minimize rotational resistance and hinge friction at the cantilever ends.

The G_{IIC} test was carried out according to DIN EN 6034, and the samples were manufactured from the DCB specimens used for G_{IC}. For the G_{IIC} testing, a 100 kN universal testing machine adapted for cryogenic testing was used, designed by Franz Wohl + Partner Prüfmaschinen GmbH (Schalkau, Germany). A metallic LN2 dewar was incorporated to keep the testing under cryogenic conditions. These containers minimize heat transfer, preventing the cryogenic liquid inside from warming and evaporating too quickly. A pre-load of 50 N was required when filling the LN2 reservoir, so the sample is in the aligned position and not affected by the boiling of LN2. A load on the specimen was applied with a crosshead displacement rate of 1 mm min^{-1}. The testing setup can be seen in Fig. 3. Preliminary tests using a PT100 temperature sensor indicated that the specimens cooled down rapidly, reaching 77 K within just a range of seconds. At least 5 specimens were measured for each system, in each given testing temperature, for each testing mode.
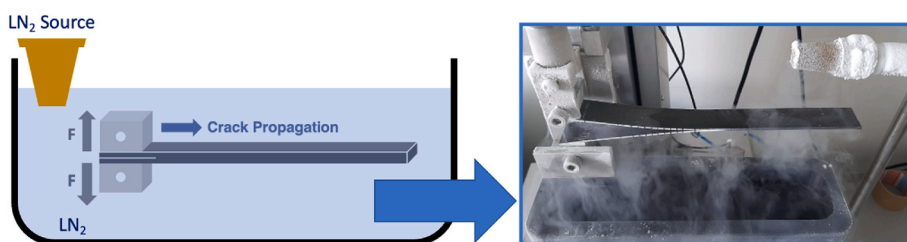

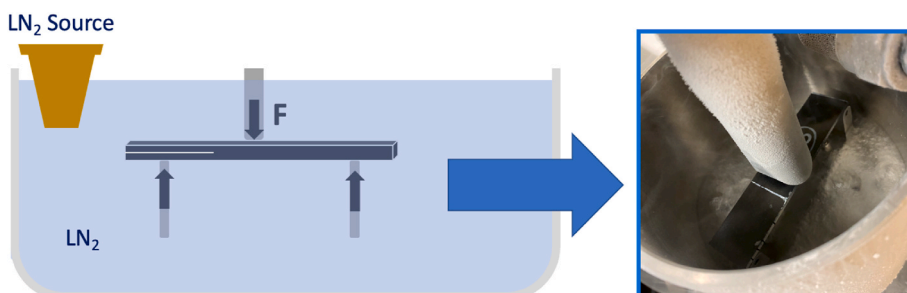**Fig. 2.** Energy release rate mode I (G_{IC}) adapted setup for DCB specimen at 77 K.

Fig. 3. Energy release rate mode II (G_{IIC}) adapted setup for DCB specimen at 77 K.
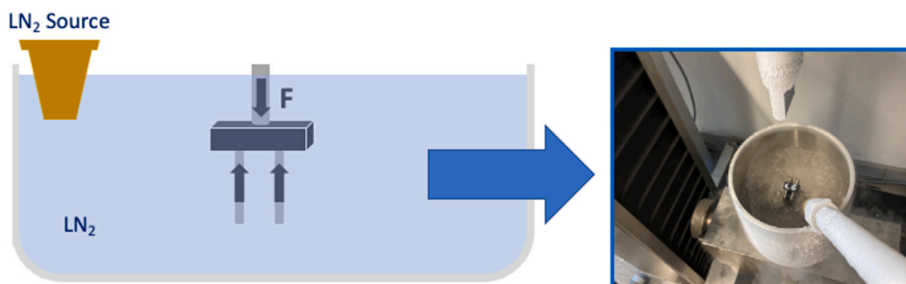
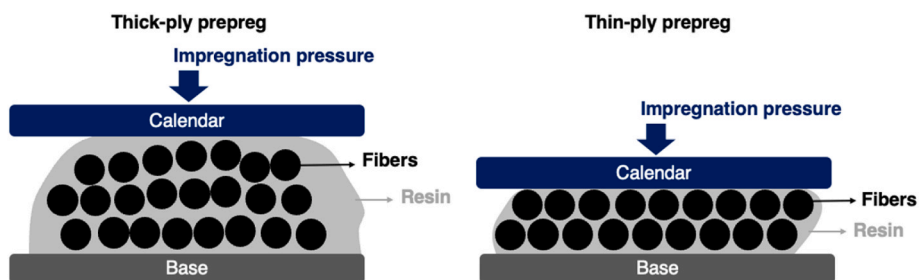**Fig. 4.** Short beam shear method adapted for ILSS testing at 77 K.

**Fig. 5.** Schematic view of prepreg spreading process from thicker to thinner plies.

2.3. Interlaminar shear strength

Short beam shear method was carried out *in-situ* LN2 to determine the ultimate shear strength of the CFRP systems in cryogenic environments. For this test, the 100 kN universal testing machine was similarly adapted as the setup shown in Fig. 3 (G_{IIC}), where a metallic dewar surrounded the test environment under LN2. A load on the specimen was applied with a crosshead displacement rate of 1 mm min^{-1}. The test followed the standard DIN EN ISO 14130. The adapted testing setup can be seen in Fig. 4. A total of 10 specimens were measured for each system, in each testing temperature.

2.4. Microscopy and fractography

An optical microscope Leica DM6000 was used to observe the structural regularity and homogeneity of the different ply thickness laminates after autoclaving. ILSS specimens were cut and used (without any testing) to observe the regularity of fiber-resin distribution and overall homogeneity of the layers. Moreover, ILSS specimens were observed in the optical microscope after testing in RT and 77 K, seeking to observe the failure behavior. The fractured longitudinal section of the G_{IC} specimens tested at both RT and 77 K environments was examined using a Zeiss Gemini 1530 SEM. Before examination, the surfaces were platinum-sputtered to a thickness of approximately 5–10 nm. The SEM was operated at a voltage of 3 kV.
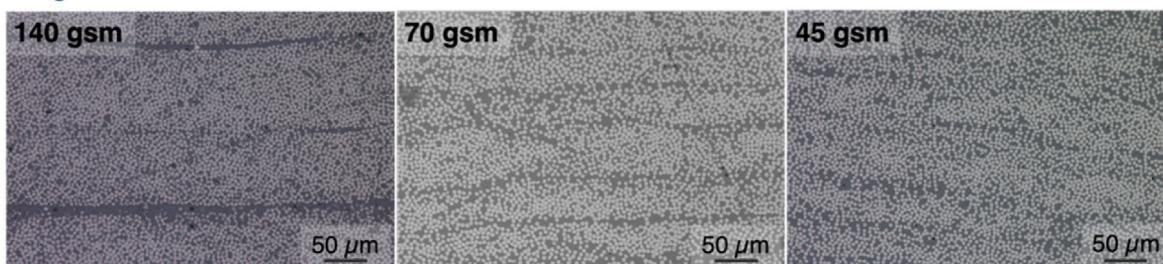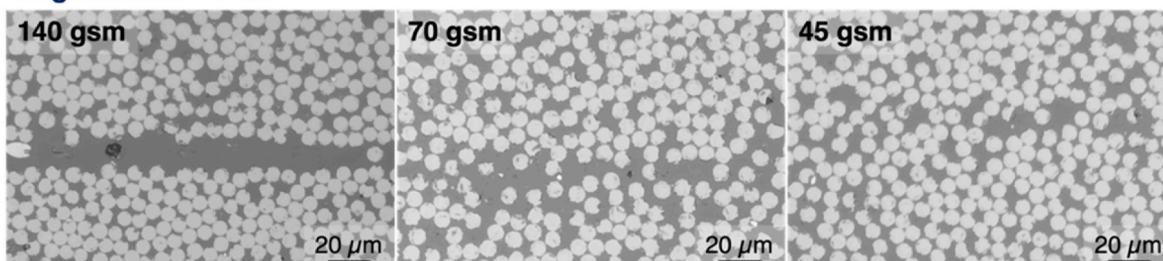

Fig. 6. Optical microscopy cross-section view of ILSS specimens prior to testing.
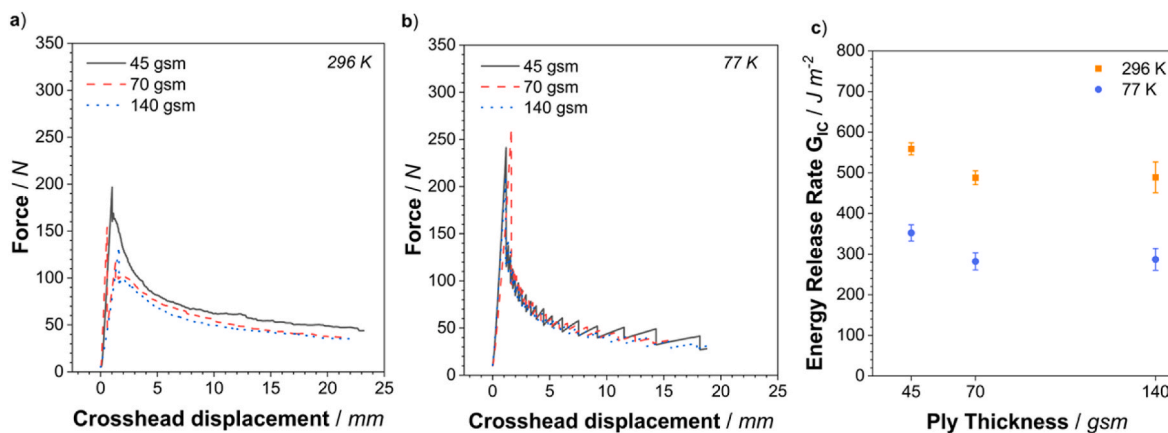
Fig. 7. Force-displacement representative G_{IC} curves for CEP-IMA laminates in different ply-thickness at a) 296 K testing, b) 77 K testing, and c) the calculated average G_{IC} values.

3. Results and discussion

3.1. Effect of process on prepreg regularity

The manufacturing process of composite parts is not entirely independent of scale. Various factors such as residual strains, fiber alignment, waviness, porosity, and the presence of fiber clustering and resin-rich zones tend to magnify in larger and thicker structures. This phenomenon introduces a distinct size effect closely tied to the production process. By spreading the fibers further during processing, a reduction in accumulated layers of resin- and fiber-rich areas is usually seen, as further pressure is applied to impregnate the resin into a thinner layer of fibers. This results in a more uniform distribution of fibers throughout the matrix. This is especially true for high-viscosity resins designed for the automated fiber placement (AFP) process. The rheological behavior of the resin governs its free-flow for impregnation. If the resin is too low in viscosity, it can lead to resin bleed, leaving dry spots behind. Conversely, if the resin is too tacky, it may result in resin being embedded without adequately covering all prepreg areas. An illustration of the effect of thin- and thick-ply impregnation can be seen in Fig. 5. Note that as the prepreg ply becomes thicker, there is a stronger tendency for the film shape to become less flat (elliptical) rather than maintaining a flat, film-like shape. Depending on the resin viscosity, these resin-rich zone spots will not spread unless sufficient pressure is applied with the impregnation calendar. The advantage of high-tackiness resin for thin-ply spreading is that the fibers are dragged further to the sides as they strongly cohere to the resin film. Another important feature regarding the processing is the gap between carbon-fibers within the width of the tape after impregnation, which tends to concentrate more when the spreading force is unequal along the width. These regions will likely be susceptible to a fiber-rich zone. By spreading further the fibers within the tape, the likelihood of this scenario is reduced.

To observe the laminate microstructure evolution as the ply thickness is reduced, a cross-section view from optical microscopy of the cured laminates is shown in Fig. 6. Such pronounced differences in microstructure shed light on the relatively inferior performance of thick ply specimens shown by Refs. [29,30] compared to the thinner ply laminate. Analyzing the microscopic images, it is possible to see very well-defined resin layers at the ply interface. At higher magnification, the accumulated resin lines are seen very clearly and more present in the 140 gsm laminate, on a range of 10–20 μm thick. These resin pockets are seen to decrease at 70 gsm, and further to less than a carbon-fiber diameter thickness (<5 μm) at 45 gsm.

The analysis of FVC variation through TGA experiments revealed a significant difference between thicker and thinner plies, specifically when comparing 140 gsm and 45 gsm laminates. The thicker-ply laminate exhibited a notable heterogeneity with FVC varying by ±4 vol%, while the thinner-ply laminate showed a much more uniform FVC distribution, with only ±1 vol%. The TGA specimens had a cross-sectional area of approximately 1 mm × 1 mm. Given the resin pockets of about 20–30 μm seen in the 140 gsm system (see Fig. 6), it can be assumed that specimens containing more of these pockets will exhibit significantly lower FVC than those without. Thus, this variation can also be attributed to the length scale of the specimens. Nevertheless, such variation can negatively impact the mechanical properties of the laminate, making it more susceptible to premature failure, especially in resin-poor regions where fiber-matrix interface density is higher, and cracks are more likely to initiate.

3.2. Intralaminar toughness

The interlaminar fracture toughness values measured through peel-force as a function of the crosshead displacement are shown in Fig. 7a and b, as a representative average curve of each CEP-IMA system, at 296 K and 77 K testing, respectively. Notice here that the crosshead displacement is later converted to crack length, so the release energy can be calculated. A summary of the G_{IC} results in 296 K and 77 K environments is provided in Fig. 7c. As outlined in Section 2.2, the measurements are initially recorded as force vs. crosshead displacement (Fig. 7a and b). During the test, the machine's crosshead displacement values are converted into crack length at the specimen. The energy release rate G_{IC} is then calculated using Zwick® software by evaluating the triangular areas under the force vs. crack length curve (already converted) and determining an average G_{IC} value. Notice here, the force-displacement curve for mode I cannot be used to assess stiffness or modulus until the crack length exceeds 50 mm (here located in the range of 4–6 mm of crosshead displacement), as initial data may be influenced by adhesive covering the end-notch. Beyond this threshold, the curves converge, providing reliable data (see DIN EN 6033).

For RT testing, notice that the force required to delaminate the CFRP material increases slightly as the ply thickness decreases. The thinner-ply laminates offer an increase in structure regularity and fiber distribution (e.g. minimization of fiber-rich zones), thus providing a more homogeneous stress allocation and further toughness on the delamination process. The fiber-rich areas are considered to worsen the delamination toughness by decreasing the resin volume area, leading to less potential elastic deformation. This reduces fiber bridging and peeling force, thereby lowering the overall delamination energy. This phenomenon is evidenced by Riccio et al. [30], who demonstrated the correlation between increased FVC and diminished fiber bridging in composite materials.
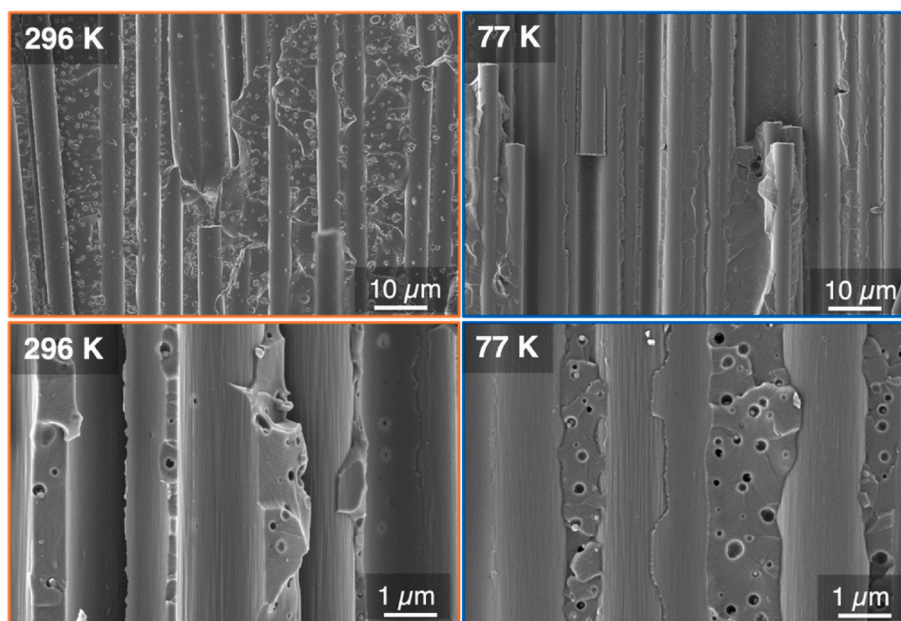
Fig. 8. SEM images of fractured G_{IC} 70 gsm specimens after 296 K and 77 K testing at 500 × (top) and 5000 × (bottom) magnifications.
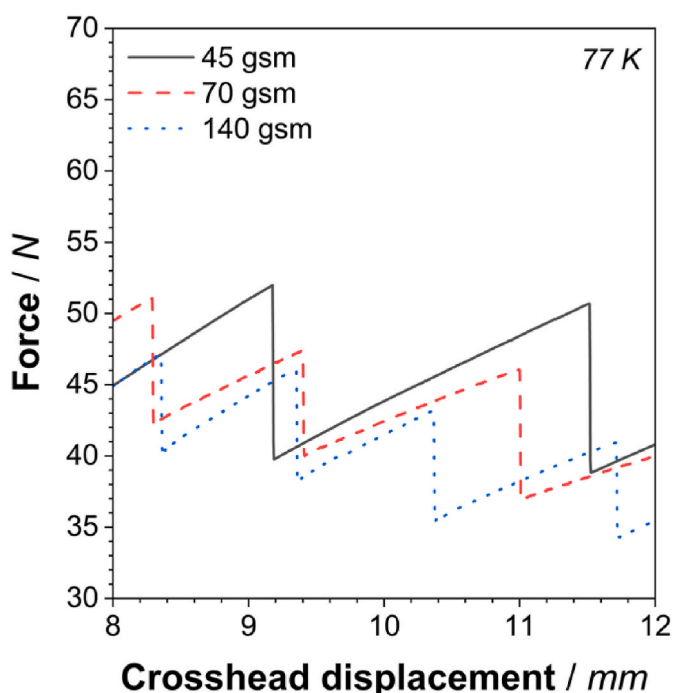

Fig. 9. Approximated view of the G_{IC} force vs. crack displacement representative curves at 77 K testing derived from Fig. 7b.

In cryogenic environments, the rapid crack propagation poses a challenge for testing equipment to synchronize crosshead speed with crack displacement, resulting in fluctuations as the crack advances. Either way, the laminate becomes stiffer, and some authors reported an increased fracture toughness of the neat resin itself [19–21], which would inherently suggest a significant increase in the peel-force required to delaminate the CFRP specimen. However, the embrittlement here causes the crack to displace with less energy dissipation, suppressing the plastic zone radius for intralaminar crack resistance, resulting in a lower energy release rate. This could also relate to the much rougher surface seen in RT fracture, whereas cryogenic surface fracture is rather smooth,

as revealed by the SEM images in Fig. 8. Here, the size of the resin debris of fracture surfaces is seen to decrease at 77 K. Additionally, it is expected that the shrinkage of the matrix around the fibers creates significant stress, further reducing the local strain failure. This phenomenon is thoroughly discussed by Sápi [3], comparing the coefficient of thermal expansion of resins and fibers.

When comparing RT and 77 K tests, distinct delamination behaviors emerge. RT tests demonstrate a matrix-dominant gradual delamination process, while at 77 K, delamination becomes unpredictable and intermittent. The fibers are seen to be far more disrupted at RT testing than at 77 K testing, resulting in higher energy required for delamination. These factors match the transition reported by Shindo et al. [13], claiming that the matrix cracking fracture behavior has a significantly lower energy level compared to matrix debonding and fiber pull-out. This could be an explanation for why the values of G_{IC} were so much lower at 77 K. The increased incidence of fiber breakage observed at 77 K suggests that the fibers indeed experience residual stress from the ultra-low temperature, making them more susceptible to fail during delamination rather than engaging in fiber bridging. No difference in fractography was detected within the SEM images in different ply-thicknesses laminates.

Despite minor deviations, the improvement from structural regularity is significant given the challenges of toughening epoxy resin for cryogenic conditions. In a closer view of the curve displayed in Figs. 7b and 9 shows an increase in force-displacement product as segments of area. The sum of these increments is associated with the increase in the G_{IC} value measured at 77 K. As long as no defects are present to propagate the crack further, the growth of these peaks can be interpreted as a toughening mechanism for the CFRP composite, particularly at 77 K, evidenced by the reduction in ply thickness.

Shindo et al. [12,13] observed that the fatigue delamination rate in mode I GFRP woven laminates is significantly lower at 77 K compared to RT. This reduction in delamination growth could attributed to the stiffening of the matrix and an increase in fracture toughness at lower temperatures (this one reported by Hübner et al. [19–21], which helps to control crack growth during cyclic loading). In contrast, at RT, the lower stiffness of the matrix offers less resistance to stress, leading to higher crack growth rates under similar conditions. However, during static testing, where the stress level grows up to failure, the reduced ductility at 77 K is thought to have far more influence on the crack length, thus decreasing the calculated G_{IC} energy product.
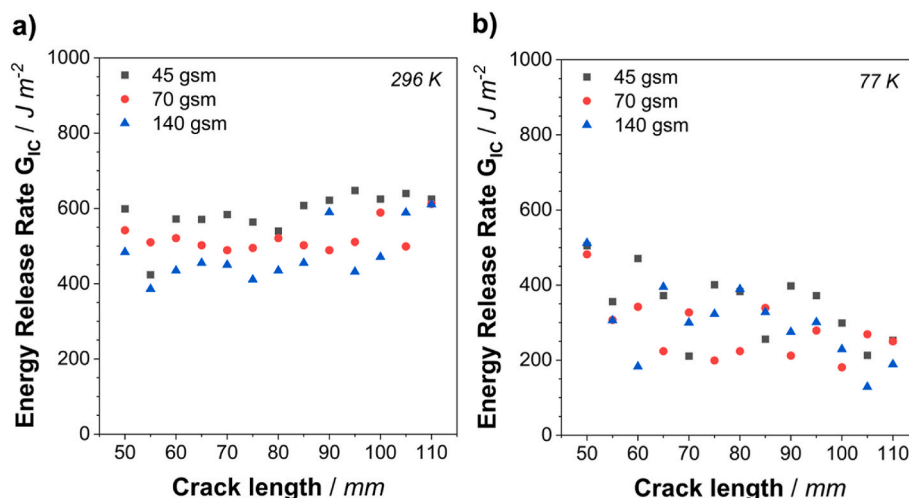
Fig. 10. Representative delamination resistance curve at a) 296 K and b) 77 K testing.
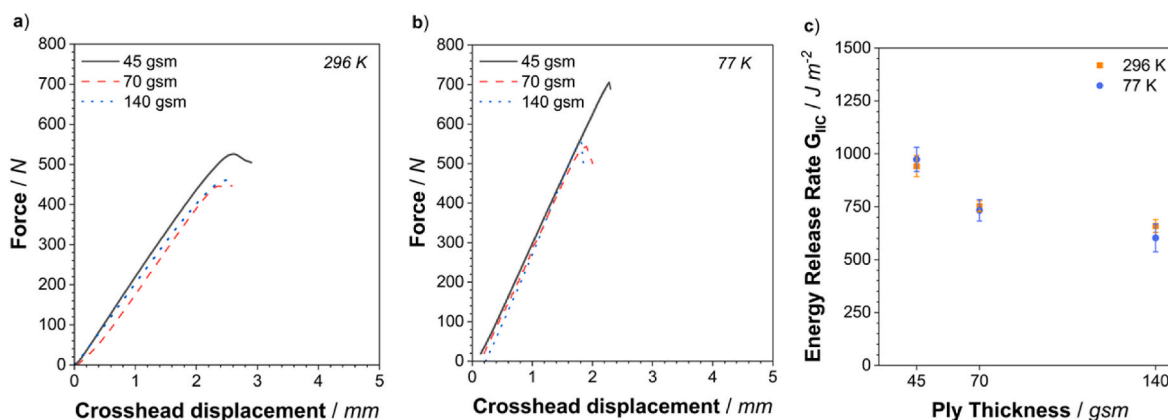

Fig. 11. Force-displacement representative G_{IIC} curves for CEP-IMA laminates in different ply-thickness at a) 296 K testing, b) 77 K testing and c) the calculated G_{IIC} values.

The delamination resistance curves as G_{IC} vs. crack length are shown in Fig. 10 for the representative specimens (respective shown in Fig. 7) tested at 296 K and 77 K. Each representative plot includes data from the start of crack growth at 50 mm through to 110 mm. The role of these resistance curves (R-curves) is to assess the stability of crack propagation. A positive slope in the R-curve suggests that the material becomes more resistant to crack growth as the crack extends. This is typical of tough materials, which can dissipate more energy as the crack progresses. On the other hand, a negative slope is usually observed in brittle materials, indicating that once the crack initiates, it propagates more easily, increasing the likelihood of sudden failure.

For the tests at RT, a slight positive R-curve is observed, indicating an increase in G_{IC} as the crack length extends. This trend is consistent across all ply thicknesses. This positive slope is primarily attributed to fiber bridging, fiber-matrix debonding, and fiber pull-out, which remain more consistent as the crack grows. This aligns with the features observed in the SEM images (Fig. 8). The CEP resin, designed for cryogenic environments, displays a ductile behavior at RT. Notably, the 45 gsm system shows higher breakdown G_{IC} values compared to the 140 gsm, resulting in a higher overall average of G_{IC}.

At cryogenic temperatures, the behavior changes significantly. The data points become more irregular, reflecting the unstable, brittle crack propagation observed in the force vs. crosshead displacement curves. When the crack displacement mark aligns with a force peak, the G_{IC} obtained there is higher, but it is lower when the mark falls between peaks. For all ply thicknesses, the breakdown G_{IC} values are scattered between peaks and valleys. More importantly, the R-curve shows a slight negative slope, which is unfavorable for delamination, supporting the idea that the matrix becomes brittle at 77 K. Initiation values are somewhat higher but tend to decrease as the crack grows. Similar findings were reported by Johnson et al. [8], who measured R-curves for an 8- and 16-ply IM7-977-2 system (a relatively brittle matrix). At cryogenic temperatures, it was observed a clear negative slope due to the material's low delamination resistance. At RT, it was reported a relatively flat R-curve for both ply thicknesses.

Different from mode I, mode II delamination toughness G_{IIC} measures the energy release rate through the composite via shear forces at the crack tip. In Fig. 11a and b, the representative curves of G_{IIC} force vs. crosshead displacement are plotted for 296 K and 77 K testing, respectively. The values of GIIC were calculated as a function of the maximal load and geometry of the specimen (see DIN EN 6033), summarized in Fig. 11c.

The impact of matrix stiffening on Mode I fracture toughness (G_{IC}) is notably more pronounced than on Mode II (G_{IIC}). This distinction arises from the fact that Mode II primarily considers the first-crack-propagation rather than a crack propagation length. While G_{IC} is highly sensitive to embrittlement effects, the cryogenic temperature unbalances the product between force/crack displacement. Conversely, G_{IIC} balances stiffening and embrittlement, leading both RT and cryogenic tests to yield nearly identical results. Furthermore, the laminate
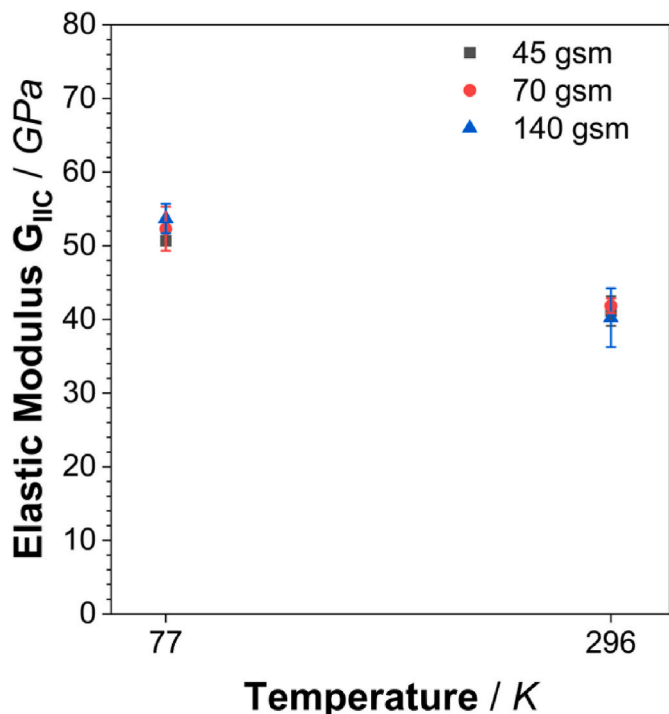
Fig. 12. Calculated elastic modulus *E* from G$_{IIC}$ curves at 296 K and 77 K for the different CEP-IMA ply-thickness systems.

ply thickness significantly influences the values of G$_{IIC}$, as seen in G$_{IC}$. Thinner-ply interface is described by Ref. [26] to reduce transverse shear stress between adjacent layers. This seems to be even more pronounced in cryogenic environments, as levels of residual stress is believed to rise substantially over the course of the temperature range [3,4].

The force-displacement curves, in addition to reflecting differences in slope caused by variations in sample geometry, also suggest that FVC within the representative specimens varies. This is consistent with the greater deviation observed in the G$_{IIC}$ calculated values (which are normalized by the geometry), providing further insight into the influence of FVC on the results. Specifically, The TGA results showed greater variability in the FVC for the 140 gsm system. Therefore, it is likely to see a greater deviation in the stiffness of the curves. In specimens where the structural regularity and fiber distribution are more homogeneous, the likelihood of significant deviations in the force-displacement curve is

reduced. This observation aligns with the lower standard deviation seen in the G$_{IIC}$ values for 70 and 45 gsm specimens, reflecting a more consistent mechanical behavior.

At RT, the G$_{IIC}$ specimens testing of CFRP composites shows stable crack growth due to the ductile and tough resin matrix, which allows significant deformation and elongation. The resin specifically designed for 77 K is characterized by low modulus and high levels of elongation, thus containing crack propagation within the plastic zone radius. In contrast, at cryogenic testing the resin becomes stiffer and more brittle, leading to unstable crack propagation, similar to what is observed in Mode I testing. This shift in behavior is consistent with literature indicating increased matrix stiffness and embrittlement at low temperatures, resulting in more brittle failure modes, as brought by Refs. [3,4].

A comparison of the material stiffness at 296 K and 77 K was carried out from the intralaminar toughness tests G$_{IIC}$. The relationship between the stiffness *k* and the elastic modulus *E* can be expressed as described in the European Structural Integrity Society (ESIS) TC4 protocol for Mode II intralaminar fracture toughness of unidirectional fiber-reinforced polymer composites [31]:

$$E = \frac{k \bullet (L^3 + a^3)}{8 \bullet b \bullet h^3} \, Eq \qquad (1)$$

Where *L* is the setup span of the testing, *b* and *h* are width and thickness of the specimen, respectively, and *a* is the end-notch length. The values of stiffness *k* were determined within the linear elastic region of the measured specimens. The values of *E* were calculated with the *h* values found in Table 2, and the geometry values of *L* and *b* folllow the standards DIN EN 6034 (G$_{IIC}$) varying slightly depending on each system. Finally, the calculated *E* values at RT and 77 K considering all systems are shown in Fig. 12.

The elastic modulus values are seen to be independent of the ply thickness, considering a small deviation (here likely attributed to FVC and thickness variation). This is expected as the elastic modulus is a parameter governed by the individual properties of matrix and fiber. The increase in the elastic modulus values by the decrease in the temperature, in the range of 15–20 %, again indicates the rise in laminate stiffness at ultra-low temperatures. Such a behavior is commonly reported by several authors [4,5,11–14].

3.3. Interlaminar shear strength

A representative ILSS curve of force vs. displacement for each ply-thickness system can be seen in Fig. 13 at RT testing. Here, notice the significant plastic deformation being carried by the tough epoxy matrix. Commonly, matrix failure and crack propagation along the near axial
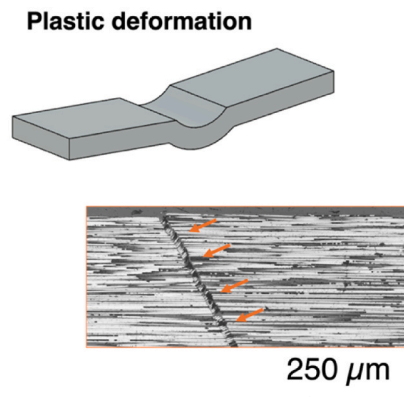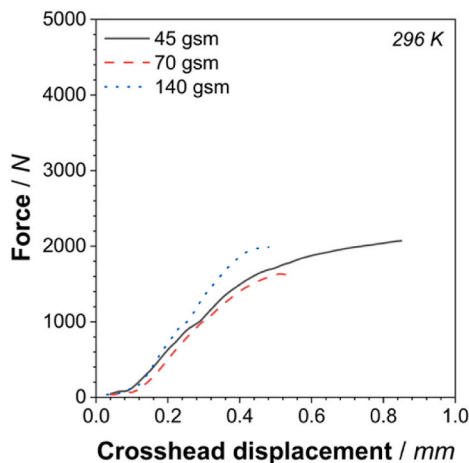

Fig. 13. Representative curves of force vs. displacement of ILSS specimens with different ply-thickness at 296 K, an illustrative, and a microscopic longitudinal-section image of a representative specimen exhibiting non-shear failure.
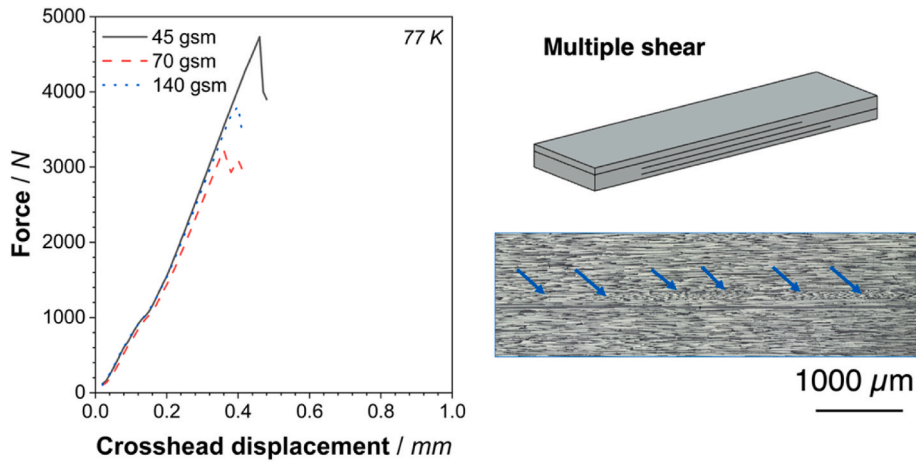
Fig. 14. Representative curves of force vs. displacement of ILSS specimens with different ply-thickness at 77 K, an illustrative, and a microscopic longitudinal-section image of a representative specimen exhibiting shear failure.
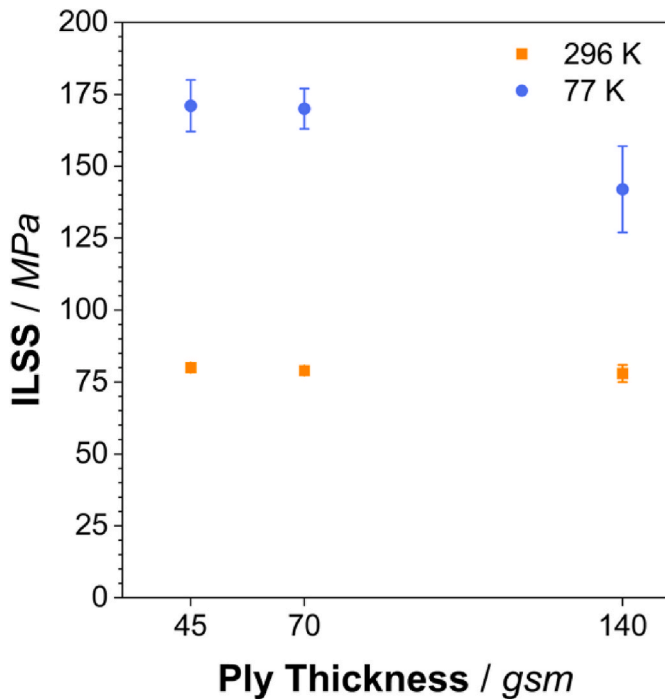

Fig. 15. ILSS calculated values for CEP-IMA laminates as a function of the ply-thickness at 296 K and 77 K.

Fig. 16. Radar chart of all measured properties at RT and 77 K for the different ply-thickness CEP-IMA laminates.

direction lead to interface weakening, provoking shear failure. Since the matrix is considered the weakest part of the composite structure, it is assumed that crack initiation would take place from defects or voids normally expected to be more present in thicker ply laminates. However, due to the significantly large plastic zone radius (as demonstrated by Ref. [20], the cryogenic resin herein exhibits a plastic zone radius of 24.1 µm at RT, whereas common epoxy systems are in the range of 12.0 µm), the failure of the specimen is rather through plastic deformation than shear itself. As a result, crack is initiated from extensive compression of the neutral surface rather than along the near axial direction. Thus, no true shear stress at failure. The attached microscopy of the ILSS specimen after failure exhibits signs of kink-band formation and transversal failure rather than longitudinal shear failure. The type of failure was seen independent of the ply thickness. Even though values of force and displacement vary, the values of ILSS for RT testing were in a very close range (averaged and normalized by the specimen thickness). In RT
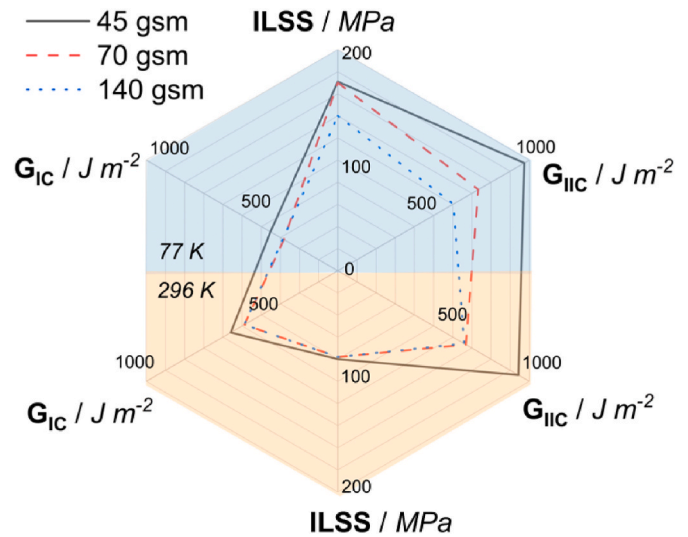
testing, no effect of the ply thickness on the ILSS value of the CFRP laminate was found. Amacher et al. [29] also reported no enhancement in ILSS values by decreasing the laminate ply thickness at RT testing.

A similar analysis was done in Fig. 14 for the force vs. displacement of ILSS specimens tested in cryogenic environments, for the different ply-thickness systems. The shear behavior of CFRP laminates is primarily governed by the matrix. As mentioned previously, the epoxy matrix at 77 K experiences an increase in stiffness and strength, accompanied by a decrease in the failure strain. Hübner et al. [19] reported an increase of 100 % in the epoxy resin storage modulus when switching from RT to −150 °C. Thus, suggesting that the CFRP laminate ILSS values tend to increase in lower temperatures accordingly. Different from RT testing, the stiff matrix now drastically decreased the plastic zone radius (measured as 1.4 µm at 77 K compared to the 24.1 µm at RT for this resin [20]), resulting in a significantly lower plastic deformation of the matrix. Therefore, the specimen now exhibits several shear plane failures approximately at the neutral fiber axis, susceptible to damage initiation at the interlaminar region. Important is that, at this type of failure, structural regularity and fiber-rich zones might take the lead on damage initiation. Thus, due to the accordingly mentioned process irregularities of thicker plies, 140 gsm laminate exhibits lower ILSS values when compared with 70 and 45 gsm laminates at this

Table 3
Summary of G_{IC}, G_{IIC}, and ILSS results measured at 296 K and 77 K testing.

Testing	296 K			77 K		
	45 gsm	*70 gsm*	*140 gsm*	*45 gsm*	*70 gsm*	*140 gsm*
G_{IC} $J\,m^{-2}$	559 ± 15	488 ± 17	489 ± 38	352 ± 45	282 ± 21	287 ± 27
G_{IIC} $J\,m^{-2}$	942 ± 51	668 ± 33	659 ± 30	974 ± 58	733 ± 51	603 ± 66
ILSS MPa	80 ± 1	78 ± 1	78 ± 3	171 ± 8	170 ± 7	142 ± 15

temperature regime. The attached microscopy image displays the aforementioned type of failure.

The calculated ILSS values tested in both 296 K and 77 K are shown in Fig. 15. Here, the curve discloses that the mode of failure is directly related to whether the material can be improved by the regularity of the laminate's microstructure or not. The significant deformation in RT environments permits the laminate to fail mostly independent from irregularities and heterogeneities (e.g. resin-fiber-rich zones), as plastic deformation takes over the laminate at a macrostructural level (non-shear failure). On the other hand, a completely different mode of failure is demonstrated in a cryogenic regime (shear failure). The suppression of plastic deformation and thus increasing sensitivity to defects highly points out the enhancement of thin-ply laminates towards shear strength. Here, as failure is contained at a microstructural level, irregularities increase their role significantly.

Finally, the radar chart in Fig. 16 summarizes the results obtained through this study, considering interlaminar energy release rate (mode I and II) and interlaminar shear strength across different ply thicknesses (45 gsm, 70 gsm, and 140 gsm) tested at RT and 77 K. A noticeable trend is observed across the radar chart: As the ply thickness decreases, there is a gradual improvement in the measured properties. This improvement is particularly evident under cryogenic conditions, suggesting significant benefits of thin-ply laminates for cryogenic performance. Although the impact of reducing ply thickness at RT is less pronounced, it still demonstrates improvements. Table 3 summarizes the calculated G_{IC}, G_{IIC}, and ILSS values for each CFRP system at RT and 77 K testing.

4. Conclusions

In this study, the effect of the ply thickness on the intralaminar delamination and shear failure behavior of CFRP composites was analyzed in RT and cryogenic environments (*in-situ*), targeted for LH2 storage tank applications. A detailed correlation was found between the effect of the prepreg process on the laminate structure and its subsequent impact on the mechanical performance of the laminate composite in these environments. The key findings here as listed as:

The manufacturing process of thick- and thin-ply prepregs significantly affects the structural regularity and homogeneity of CFRP composite laminates, as observed in the microscopy images. Thicker prepreg plies are more prone to processing-related issues, such as resin pockets, fiber concentration, and overall shimmering. These effects primarily occur at a microstructural level and can significantly impact the performance of the laminate system when failure is confined to this structural range.

Intralaminar toughness in UD CFRP laminates is significantly influenced by the mode and environment of testing. The overall energy release rate G_{IC} decreases by 60–70 % at 77 K when considering the crack length. Reducing ply thickness led to a significant increase in mode I toughness at 77 K, from 282 J m^{-2} (140 gsm) to 352 J m^{-2} (45

gsm), likely due to the reduction of resin-poor areas. Similarly, mode II toughness improved from 603 J m^{-2} to 974 J m^{-2} with thinner plies, expressing even further enhancement by the homogenization of the system. However, in mode II testing, temperature effects were seen more complex. Greater deformation at RT but higher stiffness and strength at 77 K resulted in an equivalent product of strength and deformation for energy release rate mode II values. The G_{IC} R-curves demonstrated toughening behavior as the crack propagated at RT, but showed brittle behavior at 77 K, decreasing toughness as the crack displacement increased.

Shear strength is highly dependent on the behavior of the CFRP matrix, which is stiffened in the ultra-low temperature environment. The temperature transition leads to an approximate 100 % increase in shear strength, also transitioning from a non-shear failure (RT) to shear failure mode (77 K). At RT, the effect of laminate ply thickness is less pronounced, with less than a 5 % difference, as deformation extends to a macrostructural level. However, at 77 K, a 20 % increase in ILSS value is observed, suggesting that sensitivity to irregularities and defects increases as the failure mode shifts to a microstructural level.

Despite the higher cost and manufacturing challenges, thin-ply prepregs are recommended for high-performance applications requiring microstructural regularity (such as for cryogenic environments). Improvements in the laminate microstructure, including better resin-fiber distribution and inter-ply homogeneity, significantly enhance material performance. In applications like LH2 tanks for commercial aviation, where structural health is critical, delaying the onset of intralaminar/ interlaminar damage could be a key-determining matter towards product safety, making the investment in thin-ply manufacturing worthwhile.

CRediT authorship contribution statement

Eduardo Szpoganicz: Writing – original draft, Visualization, Validation, Methodology, Investigation, Formal analysis, Data curation, Conceptualization. **Fabian Hübner:** Writing – review & editing, Visualization, Validation, Supervision, Formal analysis, Conceptualization. **Uwe Beier:** Writing – review & editing, Validation, Supervision. **Matthias Geistbeck:** Writing – review & editing, Validation, Supervision. **Holger Ruckdäschel:** Writing – review & editing, Validation, Supervision, Project administration, Funding acquisition.

Declaration of competing interest

The authors declare that they have no known competing financial interests or personal relationships that could have appeared to influence the work reported in this paper.

Acknowledgement

Data availability

Data will be made available on request.

References

[1] International Energy Agency. Transport. Paris: IEA; 2022.

[2] Choi Y, Lee J. Estimation of liquid hydrogen fuels in aviation. Aerospace 2022;9.

[3] Sápi Z, Butler R. Properties of cryogenic and low temperature composite materials – a review. Cryogenics 2020;111:103190.

[4] Jörg H, Neubrand A, Fliegener S, Beckmann C, Schober M, Weiss KP, Appel S. Performance of fiber reinforced materials under cryogenic conditions—a review. Compos Appl Sci Manuf 2021;141:106226.

[5] Jörg H, Schober M, Fliegener S, Weiss KP, Appel S. Effect of cryogenic environments on failure of carbon fiber reinforced composites. Compos Sci Technol 2021;212:108850.

[6] T. T. Chiao, M. A. Hamstad, E. S. Jessop, and R. H. Toland. "Filament-wound kevlar 49/epoxy pressure vessels". (1973) n.d..

[7] Abumeri GH, Kosareo DN, Roche JM. Cryogenic composite tank design for next generation launch technology. In: Join propulsion Conference and exhibit 11-14th july 2004; 2004. Fort Lauderdale, Florida.

[8] Johnson WS, Pavlick MM, Oliver MS. Determination of interlaminar toughness of IM7/977-2 composites at temperature extremes and different thicknesses. 2005. n. d.

[9] Murray BR, Doyle A, Feerick PJ, Seprimosching COA, Leen SB, Bràdaigh CMO. Rotational moulding of PEEK polymer liners with carbon fibre/PEEK over tape-placement for space cryogenic fuel tanks. Mater Des 2017;132:567–81.

[10] Miura M, Shindo Y, Narita F, Watanabe S, Suzuki M. Mode III fatigue delamination growth of glass fiber reinforced polymer woven laminates at cryogenic temperatures. Cryogenics 2009;49(8):407–12.

[11] Miura M, Shindo Y, Takeda T, Narita F. Cryogenic interlaminar fracture properties of woven glass/epoxy composite laminates under mixed-mode I/III loading conditions. Appl Compos Mater 2013;20(4):587–99.

[12] Shindo Y, Inamoto A, Narita F. Characterization of mode I fatigue crack growth in GFRP woven laminates at low temperatures. Acta Mater 2005;53(5):1389–96.

[13] Shindo Y, Inamoto A, Narita F, Horiguchi K. Mode I fatigue delamination growth in GFRP woven laminates at low temperatures. Eng Fract Mech 2006;73(14): 2080–90.

[14] Shindo Y, Takeda T, Fumio N, Miura M, Watanable S, Koizumi N, Idesaki A, Okuno K. Interlaminar shear properties of composite insulation systems for fusion magnets at cryogenic temperatures. Cryogenics 2010;50(1):36–42.

[15] Zhao Y, Huang R, Wu Z, Zhang H, Zhou Z, Li L, Dong Y, Luo M, Y B, Zhang H. Effect of free volume on cryogenic mechanical properties of epoxy resin reinforced by hyperbranched polymers. Mater Des 2021;202:109565.

[16] Yang G, Fu SY, Yang JP. Preparation and mechanical properties of modified epoxy resins with flexible diamines. Polymer 2007;48(1).

[17] Li S, Wang H, Liu M, Peng C, Wu Z. Epoxy-functionalized polysiloxane reinforced epoxy resin for cryogenic application. J Appl Polym Sci 2019;136(2):46930.

[18] Zhao Y, Chen ZK, Liu Y, Xiao HM, Feng QP, Fu SY. Simultaneously enhanced cryogenic tensile strength and fracture toughness of epoxy resins by carboxylic nitrile-butadiene nano-rubber. Compos Appl Sci Manuf 2013;55:178–87.

[19] Hübner F, Brückner A, Dickhut T, Altstädt V, De Anda AR, Ruckdäschel H. Low temperature fatigue crack propagation in toughened epoxy resins aimed for filament winding of type V composite pressure vessels. Polym Test 2021;102: 107323.

[20] Hübner F, Hoffmann M, Sommer N, Altstädt V, Scherer A, Dickhut T, Ruckdäschel H. Temperature-dependent fracture behavior of towpreg epoxy resins for cryogenic liquid hydrogen composite vessels: the influence of polysiloxane tougheners on the resin yield behavior. Polym Test 2022;113:107678.

[21] Hübner F, Szpoganicz E, Demleitner M, Kuhnigk J, Altstädt V, de Anda AR. Time domain 1H NMR, thermomechanical, and rheology multiscale structural characterization of polydimethylsiloxane-toughened epoxy nanocomposites for liquid composite molding. ACS Appl Polym Mater 2020;2:4779–89.

[22] Kumagai S, Shindo Y, Horiguchi K, Takeda T. Mechanical characterization of CFRP woven laminates between Room Temperature and 4 K. JSME International Journal 2003;3.

[23] Shukla MD, Kumar DS, Mahato KK, Rathore DK, Prusty RK, Ray BC. A comparative study of the mechanical performance of glass and glass/carbon hybrid polymer composites at different temperature environments. IOP Conf Ser Mater Sci Eng 2015;75:012002.

[24] Surendra MK, Sharma N, Ray BC. Structural integrity of glass/polyester composites at liquid nitrogen temperature. J Reinforc Plast Compos 2009;28(11):1297–304.

[25] Sethi S, Panda PK, Nayak R, Ray BC. Experimental studies on mechanical behavior and microstructural assessment of glass/epoxy composites at low temperatures. J Reinforc Plast Compos 2012;31(2):77–84.

[26] Galos J. Thin-ply composite laminates: a review. Compos Struct 2020;236.

[27] Wu H, Li S, Zhang J, Tong L. Electrical resistivity response of unidirectional thin-ply carbon fiber reinforced polymers. Compos Struct 2019;228:111342.

[28] Sihn S, Kim R, Kawabe K, Tsai S. Experimental studies of thin-ply laminated composites. Compos Sci Technol 2007;67(6):996–1008.

[29] Amacher R, Cugnoni J, Botsis J. Thin ply composites: experimental characterization and modeling. Compos Sci Technol 2014;101:121–32.

[30] Riccio A, Russo A, Sallitto A, Toscano C, Alfano D, Zarrelli M. Experimental and numerical assessment of fibre bridging toughening effects on the compressive behaviour of delaminated composite plates. Polymers 2020;12:554.

[31] Blackman BRK, Brunner AJ, Williams JG. Mode II fracture testing of composites: a new look at an old problem. Eng Fract Mech 2006;73:2443–55.